Indian Journal of Pure & Applied Physics
Vol. 64, August 2026, pp. 853-869
DOI: 10.56042/ijpap.v64i8.30900

Analysis and Design of MCB Compliant On-Board Charger based on Topologies, Efficiency, Losses, and Automation

Arvind Kumar Singh, Jyoti Ohri & Prasad M P R*
Department of Electrical Engineering, National Institute of Technology, Kurukshetra 136 119, India

Received: 17th April 2026; accepted: 7th July 2026

This paper presents a structured design approach for an Onboard Charger (OBC) used in electric vehicles (EVs) and Marine metro vehicles, encompassing both hardware and software perspectives. The OBC architecture is typically divided into two stages the Power Factor Correction (PFC) stage and the DC-DC converter stage. For high-voltage battery charging that follows a Constant Current and Constant Voltage profile, a Boost PFC combined with a DC-DC converter controlled by an algorithm is considered an effective solution. Three PFC topologies are explored: Conventional Boost PFC, Interleaved Boost PFC, and Semi-bridgeless PFC. For the DC-DC conversion stage, the paper discusses Full-Bridge Converter, Series Resonant Converter (SRC), and Phase-Shift Full-Bridge Converter. To automate the switching operation of the Boost Converter, a Proportional-Integral (PI) controller is implemented. Beyond hardware design, the paper introduces a method to fully automate OBC operations by integrating the Renesas RH850 E2M microcontroller. This next-generation automotive power train MCU enhances the OBC with intelligent charging capabilities. Specific ECU software modules of the RH850 E2M are mapped to corresponding ECU hardware components within the OBC and the EV system. These modules enable smart features such as adaptive charging control, fault detection, and system optimization. A logical model of key ECU software modules responsible for smart charging is developed and simulated using MATLAB Simulink and Simscape. The simulation results validate the proposed design and demonstrate its potential for efficient and intelligent EV charging.

Keywords: Electric vehicles (EVs), Electric vehicle supply equipment (EVSE), On-board charger (OBC), Master control board (MCB), Power factor corrector (PFC), Series resonant converter (SRC), DC-DC converter, Controller area network (CAN), Pulse width modulation (PWM), Ziegler-nichols tuning

1 Introduction

In recent years, the demand for electric vehicles (EVs) has surged due to their efficient energy usage and zero-emission benefit[1-2]. To promote environmental sustainability, major EV-producing and consuming nations such as China and the United States are shifting their policies and market strategies toward EVs and Plug-in Electric Vehicles (PEVs), significantly expanding their EV fleets[3-5]. A critical component of EV infrastructure is the OBC, which converts grid electrical energy into stored energy within the vehicle's battery[6-8].

OBCs are preferred over traditional external chargers due to their compact size and lightweight design, making them suitable for integration within the vehicle[9]. Technically, OBC is responsible for charging high-voltage batteries that power the motor and other drive train components. The OBC circuit is typically divided into two stages: the PFC stage and the DC-DC converter stage. The PFC stage improves the power factor of the 50–60 Hz AC supply during charging, while the DC-DC converter ensures stable charging using Constant Current and Constant Voltage profiles[10-11].

This paper discusses three topologies for each stage. For PFC: Conventional Boost PFC, Interleaved Boost PFC, and Semi-bridgeless PFC. For DC-DC conversion: Full-Bridge Converter, SRC, and Phase-Shift Full-Bridge Converter. The proposed OBC design uses Conventional Boost PFC and a standard Boost Converter, with switching operations automated via a PI controller.

Further automation is achieved by integrating software ECU modules from the Renesas RH850 E2M microcontroller, enabling smart communication between the EVSE and EV components during charging. The design and simulation models are developed using MATLAB Simulink and Simscape tools. This paper presents a comprehensive design and analysis of an OBC for electric vehicles and introduces motivation and background for OBC development. This work also focuses on the analysis of various topologies and the detailed design of the PFC and DC-DC converter stages, which form the core of the OBC system[12-14].

*Corresponding author: E-mail: mprprasad@nitkkr.ac.in

An automation concept using software ECU modules from the Renesas RH850 E2M microcontroller, aimed at enhancing smart charging capabilities have been considered in this work.

To maximize battery performance and longevity, the design of an efficient and reliable battery charger is essential. Key characteristics of a high-quality charger include efficiency, reliability, compactness, cost-effectiveness, reduced charging time, and high-power density. These features are influenced by the choice of components, switching techniques, and control algorithms. The control algorithm can be digitally implemented using a microcontroller for enhanced precision and adaptability[15].

The block diagram of an onboard charger is shown in Fig.1, shows the block diagram of an EV charger, which is typically divided into two main stages. The first stage is an AC-DC converter integrated with a PFC circuit. This stage ensures a high-power factor and minimizes Total Harmonic Distortion (THD) during the charging process. The second stage is a DC-DC converter, responsible for regulating the output voltage and current to meet the battery's charging requirements.

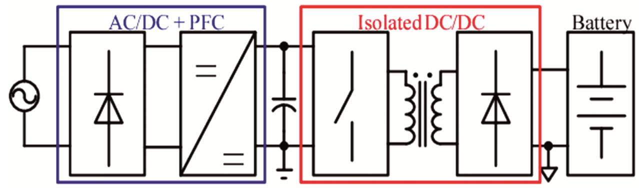

Fig. 1 — Block diagram of onboard charger

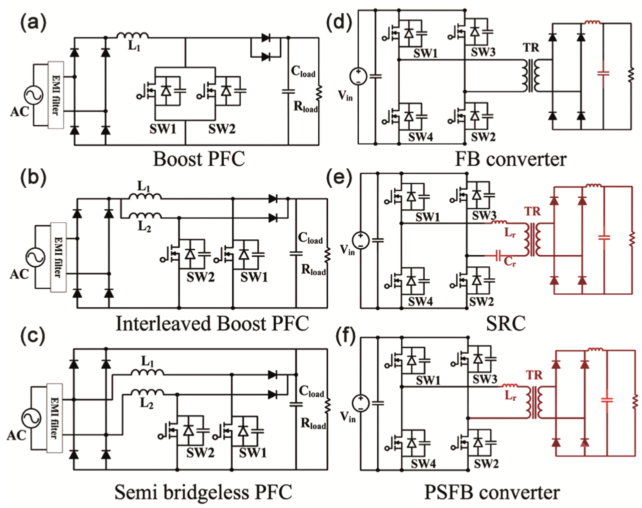

Fig. 2 — OBC's topologies (a) Boost PFC circuit (b) Interleaved Boost PFC circuit and (c) Semi bridgeless PFC circuit (d) FB Converter circuit (e) SRC circuit and (f) PSFB converter circuit

2 Topology Analysis

2.1 Topology structures

Although the OBC circuitry incorporates various topologies, achieving high performance under moderate power conditions in the PFC stage and ensuring electrical isolation between the grid and the battery in the DC-DC converter stage are critical design requirements. To meet these needs, bridge-type DC-DC converters are considered the most suitable option.

In the PFC stage, three topologies are analyzed: Conventional Boost PFC, Interleaved Boost PFC, and Semi-bridgeless PFC. For the DC-DC conversion stage, the paper discusses Full-Bridge Converter, Phase-Shift Full-Bridge Converter, and Series Resonant Converter, each evaluated based on efficiency, switching behavior, and power losses. These configurations are illustrated in Fig. 2.

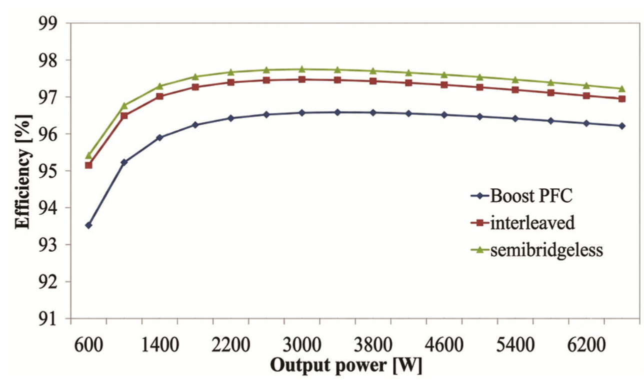

Fig. 3 — Efficiencies of PFC

Figure 3 shows the efficiency of each PFC circuits. Interleaved and semi bridgeless PFC shows higher efficiency than Boost PFC.

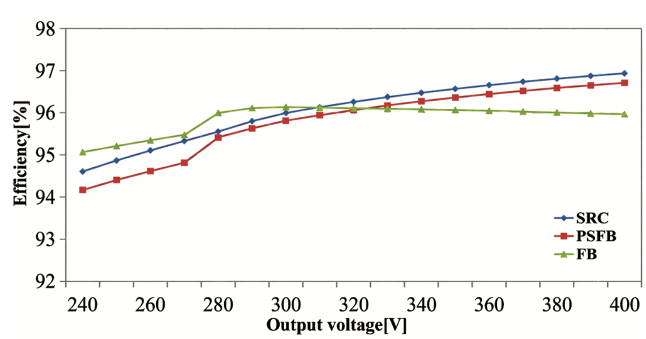

Fig. 4 — The efficiency of the DC-DC converter

Figure 4 shows efficiency performance of various DC-DC converter topologies designed for a charging voltage range between 240V DC and 400V DC, in line with battery specifications. The Full-Bridge and

Phase-Shifted Full-Bridge converters operate at a fixed switching frequency of 100 kHz. In contrast, the SRC functions over a variable frequency range from 86 kHz to 130 kHz where 86 kHz corresponds to its peak power operation and 130 kHz to its minimum power output. At lower nominal voltages, the FB converter demonstrates superior efficiency. However, at higher voltages, the SRC and PSFB converters exhibit better efficiency levels.

More elements require in case of Semi-bridgeless PFC than Bridgeless PFC. The input current ripple can reduce to half in case of both Semi-bridges less PFC and Interleaved PFC as compared with Boost PFC.

2.2 Loss Analysis

To evaluate the efficiency of various topologies used in both the PFC and DC-DC converter stages, it is essential to analyze the several types of losses that occur during circuit operation. These losses primarily arise from components such as diodes, rectifiers, and switching devices like MOSFETs and IGBTs.

Diode and rectifier losses are typically assessed based on conduction losses, which occur when current flows through the device. For switching devices, both conduction losses and switching losses must be considered. Conduction losses result from the voltage drop across the switch during its on state, while switching losses occur during the transition between on and off states due to energy dissipation. Accurate quantification of these losses is crucial for comparing the performance and efficiency of each topology.

i Conduction losses in case of diodes and rectifiers is given by;

$$P_{cond}(diode) = V_F \times I_F \times D_{on} \quad \ldots (1)$$

VF is forward voltage drop IF is conduction current, and Don is duty cycle in on condition.

ii Switch loss for switches can be defined by considering switch losses, conduction losses and losses of anti-parallel diode. Switching loss Psw is expressed by;

$$P_{sw} = 0.5 \times V_{out} \times I_{out} \times I_{rms} \times (t_{c(on)} + t_{c(off)}) \times f_{sw} \quad \ldots (2)$$

tc(on) is rise time, tc(off) is falling time, and Irms is current of the switch.

iii Conduction loss of switch is calculated by;

$$P_{cond} = I_D^2 \times RDS(on) \times D_{on} \quad \ldots (3)$$

ID is conduction current of the switch, RDS(on) is resistor at turn on condition, Loss of anti-parallel diode is calculated in Eq. (1).

The above two figures provide a detailed analysis of component-level losses across different OBC topologies. As shown in Fig. 5, both Interleaved Boost PFC and Semi-bridgeless PFC exhibit lower switching losses compared to Conventional Boost PFC. However, they incur higher losses in the inductors due to increased ripple currents and magnetic stress.

Figure 6 highlights the loss distribution in DC-DC converter topologies. The Phase-Shift Full-Bridge converter demonstrates reduced switching losses, making it more efficient in high-frequency operations. However, it shows comparatively higher losses in the inductor and rectifier components than the Full-Bridge FB and Series Resonant Converter configurations.

3 System Design

The system design of the OBC begins with the development of a Simulink model incorporating a conventional Boost PFC stage and a Boost DC-DC

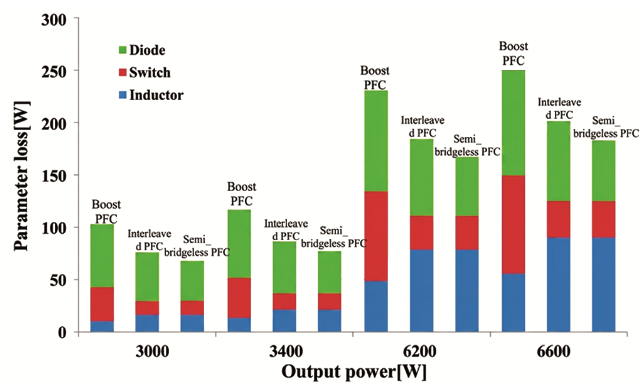

Fig. 5 — Relationship between output power and parameters of loss for PFC converters

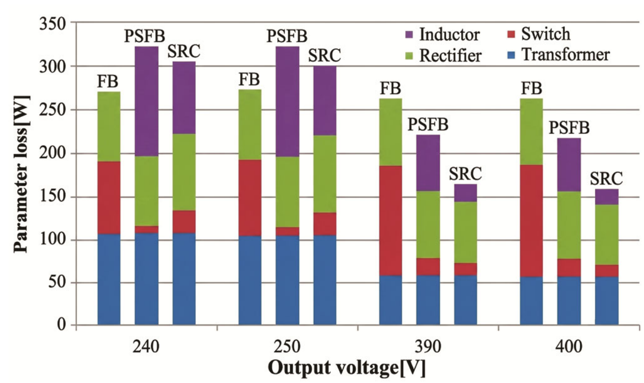

Fig. 6 — Relationship between the output voltage and parameters of loss for DC-DC converters

converter. To automate the switching operations within the circuit, a PI control algorithm is integrated into the model.

Following the hardware simulation, a logical model of selected software components from the Renesas RH850 E2M microcontroller is designed using MATLAB. These components introduce intelligent features to the OBC during the charging process, enabling enhanced control, monitoring, and adaptability. The integration of RH850 E2M software modules demonstrates how digital control can improve the overall performance and smart functionality of EV charging systems.

3.1 Conventional Boost PFC

The Conventional Boost PFC topology is one of the simplest and most widely adopted configurations in OBC design. It typically operates in Continuous Conduction Mode (CCM) at frequencies below 70 kHz, offering a balanced trade-off between ripple current and switching losses. This topology is known for its straightforward implementation and reliable performance. The conventional Boost PFC circuit diagram is shown in Fig. 7 which is essential for the OBC design.

Under optimal conditions, a Conventional Boost PFC can achieve efficiency levels exceeding 96 %, with a minor efficiency drop of approximately 1–2 % attributed to losses in the input bridge rectifier. Its simplicity and effectiveness make it a suitable choice for moderate power applications in EV charging systems.

3.2 Automated PFC and DC-DC converter

For any selected topology of the PFC and DC-DC converter stages, switching operations can be automated using a controller to implement controlled or PWM switching. In the proposed OBC model, a PI controller is employed to manage the switching of the MOSFET device, enabling precise control over the power conversion process.

When PWM-based control is applied to the PFC stage, it is referred to as Active PFC. This approach enhances power factors and reduces harmonic distortion, contributing to overall system efficiency. Figures 8 and 9 illustrate the functional block diagrams of an Active PFC and a DC-DC converter integrated with a PI control algorithm, demonstrating the control flow and interaction between components.

The procedure followed for selection of PI Controller gains is Ziegler Nichols method. It has variety of tuning methods. The ultimate gain method was used in this work.

4 Microcontroller Environment

4.1 Hardware

The Renesas RH850 E2M microcontroller is a next-generation automotive power train MCU designed for EVs, offering advanced features that enhance the functionality of the OBC during the charging process. Operating at a frequency of 400 MHz, it is equipped with high-capacity flash memory and high-speed RAM, enabling fast and reliable performance. The RH850 E2M also supports critical automotive standards, including built-in security features and functional safety compliance with ISO 26262. It has unique features like high performance Automotive MCU, high speed flash and RAM which are very much essential for Electric Vehicle Control.

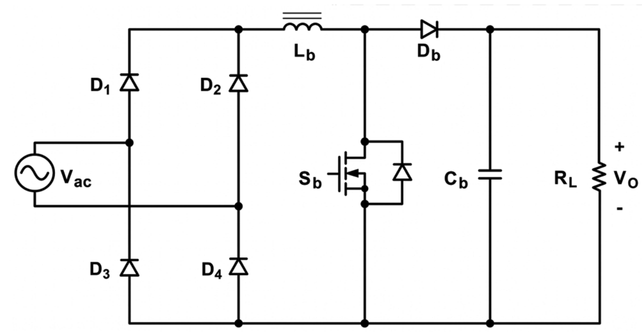

Fig. 7 — Conventional Boost PFC circuit diagram[16]

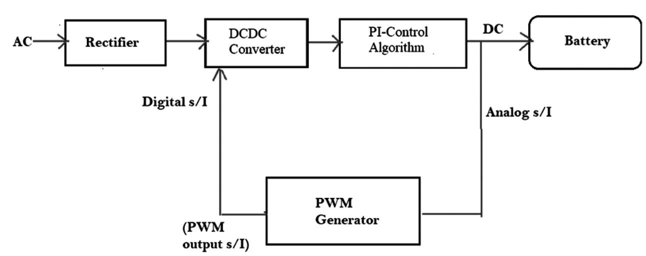

Fig. 8 — Active PFC with PI-controller

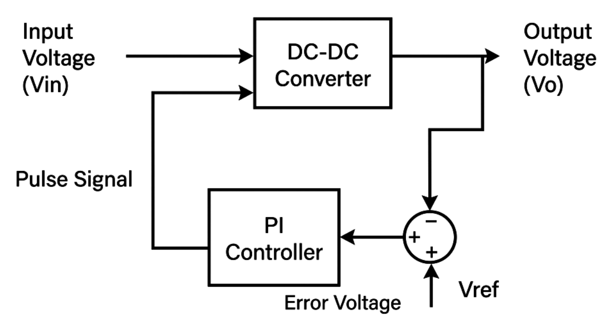

Fig. 9 — DC-DC converter with PI-controller

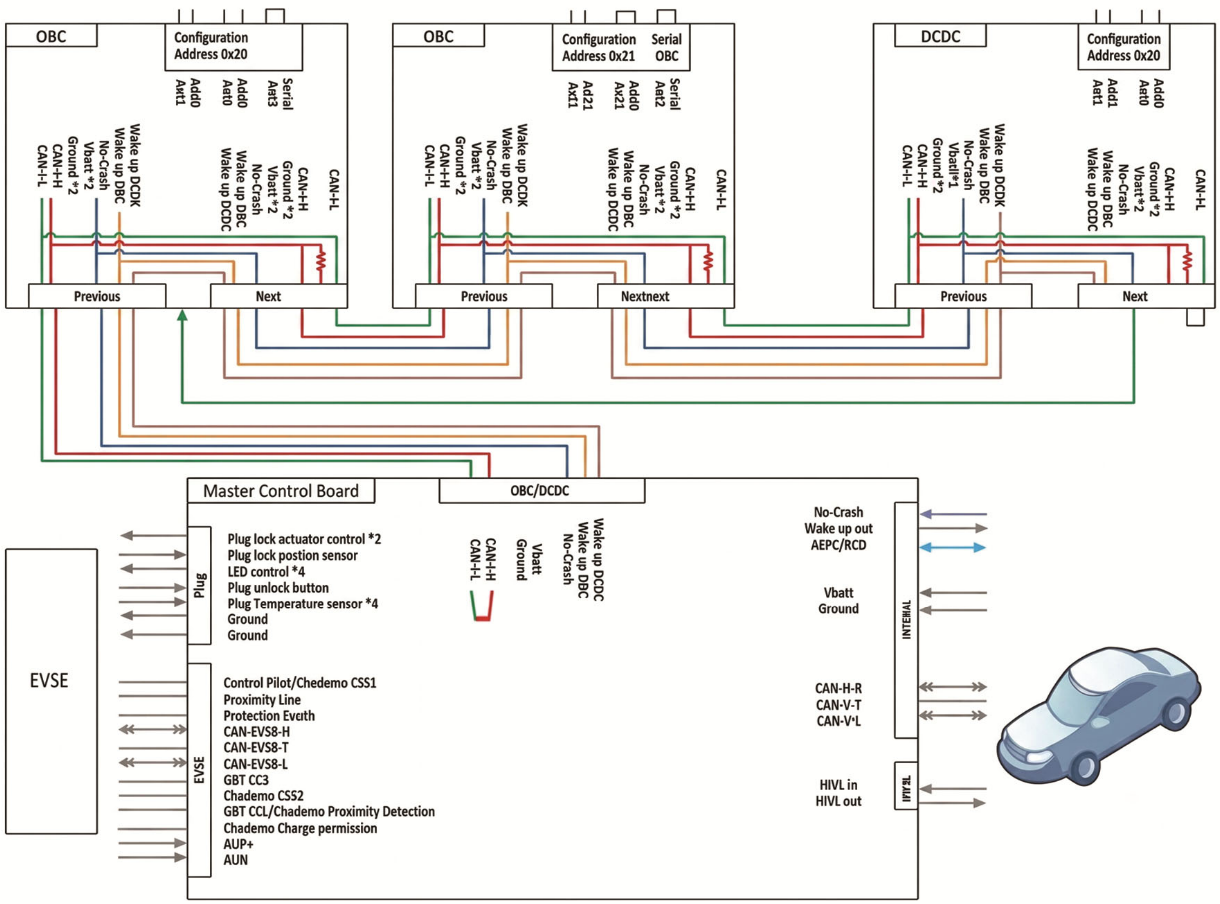

Fig. 10 — Connection configuration: 2 OBC's in series and 1 DC-DC with 1 MCB[1]

One of its key capabilities is support for Over-the-Air updates, allowing wireless software upgrades to ensure safe and up-to-date control programs without manual intervention. Communication between the microcontroller and EV hardware is facilitated through CAN protocols. The OBC and DC-DC converter interact with the microcontroller via Internal CAN (ICAN), while other major subsystems such as the Battery Management System, engine module, and driver module communicate through Vehicle CAN (VCAN). The CAN bus is a serial communication protocol that enables fast, prioritized data exchange among microcontroller-enabled devices. Data packets are transmitted sequentially, with priority given to the most critical messages.

Figure 10 explains a sample configuration featuring one MCB, two OBCs connected in series, and one DC-DC converter in parallel. Figure 11 demonstrates how the RH850 E2M MCB communicates with various EV components including the EVSE, OBC, DC-DC converter, and other hardware drivers and ECUs once initialized via the MCB wake-up line.

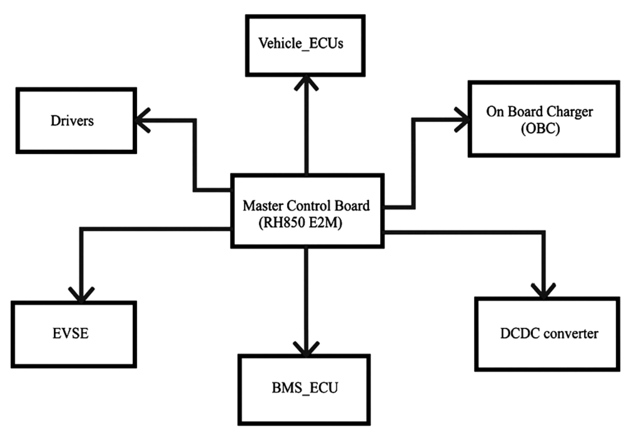

Fig. 11 — A reliable establishment of communication between RH850 E2M MCB with EVSE and EV's electronic components when MCB wakes up

The RH850 E2M electronic card shall have the following connectors (card to wire connectors) OBC/DC-DC interface, Vehicle interface, Plug interface, and EVSE interface.

4.2 Software

In automotive systems, an Electronic Control Unit (ECU) is an embedded digital controller that functions as a specialized computer. It processes signals from various sensors distributed across the vehicle and uses this data to manage critical operations such as engine control, safety systems, and automated functions.

During the EV charging process, reliable communication between the Electric Vehicle (EV) and the EVSE is essential. This is facilitated by specific ECU modules namely, the Control Pilot Module (CPM) and the Proximity Pilot Module (PPM). These circuits ensure proper signalling, safety checks, and handshake protocols between the EV and the charging station, enabling secure and efficient energy transfer. Sensors continuously track real time temperature monitoring, Adaptive charging algorithms, Constant temperature phase, constant voltage, thermal management, safety cut-offs.

The Control Pilot Mechanism (CPM) is a communication line conductor that becomes active when the EV inlet is connected to a charging connector from the EVSE. The connector, either Type 1 or Type 2, is validated through the Proximity Pilot Mechanism (PPM), which ensures proper physical connection and safety compliance. Once connected, the CPM generates a square wave signal with a frequency of 1 kHz and an amplitude ranging from -12V to +12V. This signal plays a critical role in detecting the presence of the vehicle and communicating essential charging parameters. These include the maximum allowable current, state of charge (SoC), and whether ventilation is required during the charging process.

Figure 12 illustrates the control pilot circuit line, highlighting its role in enabling safe and intelligent communication between the EV and the charging infrastructure.

Charging process begins when switch S2 is closed with CP_Voltage range 5V<=CP_Voltage<=7V on control pilot circuit line. The loads with 1.3KΩ and 270Ω ensure the condition of indoor charging area ventilation not required and required during charging.

Table 1 lists out the definition of various states that an EV/EVSE will undergo based on control pilot voltage (CP_Voltage) when the connector from EVSE is connected to vehicle charging inlet.

The control pilot circuit monitors two key parameters Control Pilot Frequency (CP_Frequency) and Control Pilot Duty Cycle (CP_Duty Cycle) to validate the charging process. If either parameter falls outside the acceptable range, the control pilot circuit signals the MCB to set a validity flag, ensuring that the charging process is halted or adjusted for safety and compliance.

These parameters are critical for confirming proper communication between the EV and the EVSE, and for enabling safe charging conditions. Figure 13 illustrates the behaviour of the control pilot monitoring system for standard connectors, including SAE J1772 and IEC 61851, highlighting their respective frequency and duty cycle specifications.

4.3 Proximity Pilot Circuit (PPM)

When the vehicle connector from the EVSE is inserted into the vehicle's charging inlet, the

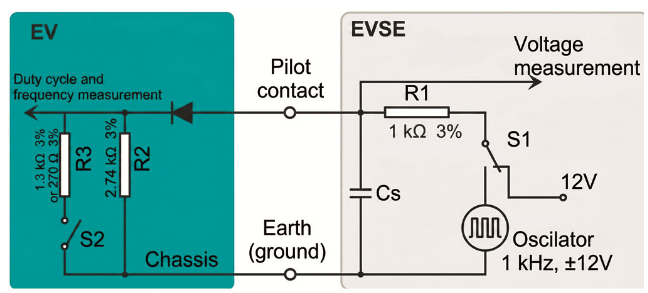

Fig. 12 — Control Pilot circuit

Table 1 — EV/EVSE States

States	EVSE (CP_Voltage)	EV (CP_Voltage)	EV/EVSE state description
A	12.0	0	Vehicle not connected
B1	9.0	9.0	Vehicle connected but not ready to accept energy / EVSE not ready to supply energy
B2	9.0	9.0	Vehicle connected but not ready to accept energy / EVSE ready to supply energy
C	6.0	6.0	Vehicle connected and ready to accept energy (no ventilation required) / EVSE ready
D	3.0	3.0	Vehicle connected and ready to accept energy (ventilation required) / EVSE ready
E	0	0	EVSE disconnected from vehicle, or CP line grounded / EVSE loses power
F	-12	-12	Error or fault condition in EVSE

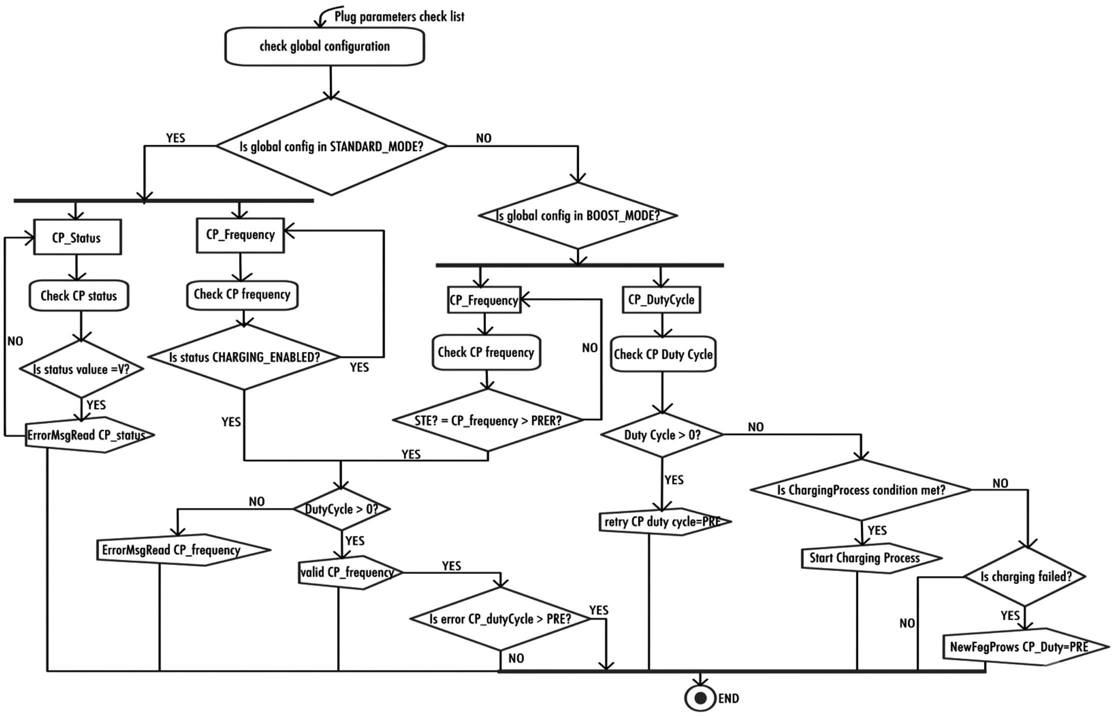

Fig. 13 — Control Pilot Monitoring for SAEJ1772 and IEC61851 standards connectors

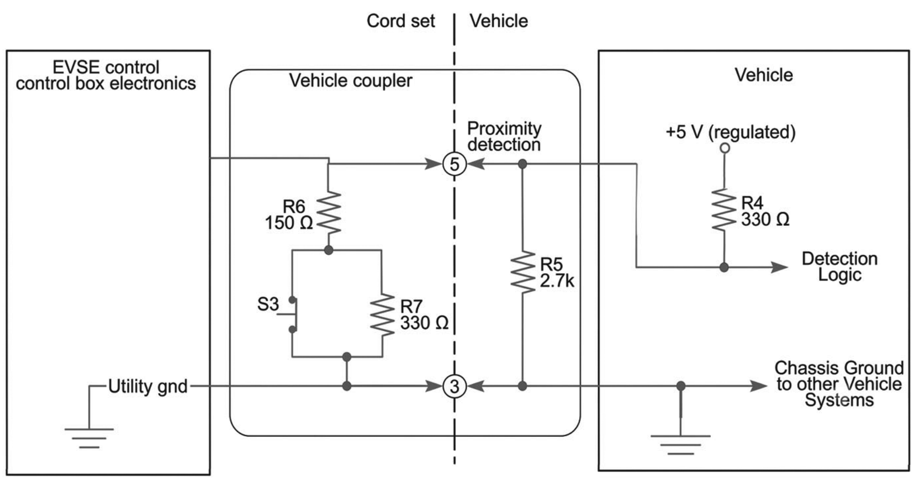

Fig. 14 — Proximity pilot circuit

proximity detection function becomes active. This is monitored through the transition of the Control Pilot voltage. Specifically, when the CP voltage drops from 12V to 6V, the proximity detection circuit confirms that the charging connector is securely engaged with the vehicle inlet.

The primary role of the proximity detection circuit is to validate the physical connection status between the EVSE connector and the vehicle inlet. According to the SAE J1772 standard, a 5V peak-to-peak signal is applied within the EV to facilitate this detection. This ensures safe and reliable initiation of the charging process by preventing unintended disconnection or unsafe operation.

The operational behaviour of the Proximity Pilot Circuit is illustrated in Fig. 14.

Proximity pilot circuit ensures that the charging connector is connected to vehicle inlet when switch S3 is closed with proximity voltage ranges 1.23V <= Proximity_Voltage<= 1.82V with no-fault occurrence detected from EVSE side. If any fault occurs proximity circuit opens S3 switch and EVSE will initiate a shutdown process by informing MCB that a fault occurs, and the system needs an immediate shutdown. Then MCB will shut down the ECU of OBC by sending it to a shutdown mode request and set OBC wakeup line to ground. Figure 15 shows the proximity of pilot monitoring behaviour for SAEJ1772 Type 1charging connectors for their different Proximity_Voltage range.

The ECU module that provides information to EV owner about plug connection status, Plug lock-unlock validation or status of switch S2 that whether it is close or not during charging is the Charging Interface module.

4.4 Charging Interface (CI)

The Charging Interface module is a composite of several software-based ECU sub modules that manage

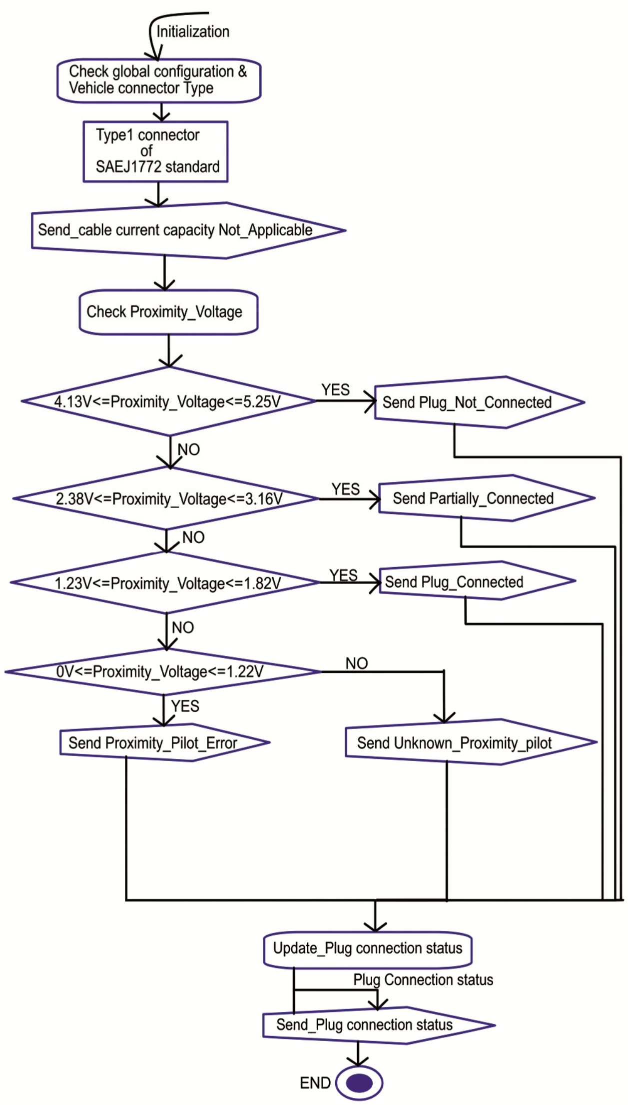

Fig. 15 — Proximity Pilot Monitoring

various aspects of the EV charging process. Among the most critical sub modules are the Proximity Pilot Mechanism (PPM), Plug Lock Status Determination, and Switch S2 Status Monitoring.

The Plug Lock Status Determination module verifies whether the charging connector is securely locked into the vehicle inlet. This validation is based on the voltage detected by the plug lock sensor. If the sensor reads a voltage within the valid range of 6V to 36V, the CI ECU sends a command to the Master Control Board to lock the plug. Conversely, if the voltage is 0V or outside the valid range, the system interprets the status as either "Unlock" or "Plug Sensor Error."

Fault conditions are also handled intelligently. For instance, if the system issues an "Unlock" command but the sensor still detects a voltage between 6V and 36V, the status is flagged as "Unlock Error." Similarly, if a "Lock" command is issued but the sensor reads 0V, the status is flagged as "Lock Error."The main challenge of Battery Management system is performance and life time. Battery Management system monitors and controls the condition of the cells, estimating battery life and protecting them from any potential threat. It gives the status of current, voltage and cell temperature.

Figure 16 presents the logic flowchart for plug lock status determination, illustrating how sensor readings and command signals interact to ensure secure and reliable charging connections.

The unlocking command within the CI module can be triggered by the Microcontroller-Based Control Block under specific conditions. One such condition is when Switch S2 is in an open state, either intentionally or due to a fault, resulting in an open error. Additionally, the charging process can be manually interrupted by pressing the unlock button located on the CI hardware module. Once the unlock button is activated, the MCB issues an unlock command, immediately halting the charging process regardless of the battery's current state of charge. This feature ensures user control and safety during charging operations in Fig. 17.

4.5 State Behavior of MCB and OBC

The OBC is initialized during the Microcontroller-Based Control Block startup or when the system enters RUN mode. Upon detecting a connection with the EVSE, the Microcontroller-Based Control activates the OBC by setting the wake-up line to the vehicle battery voltage. Immediately after initialization, the OBC enters the STANDBY state, where it remains inactive.

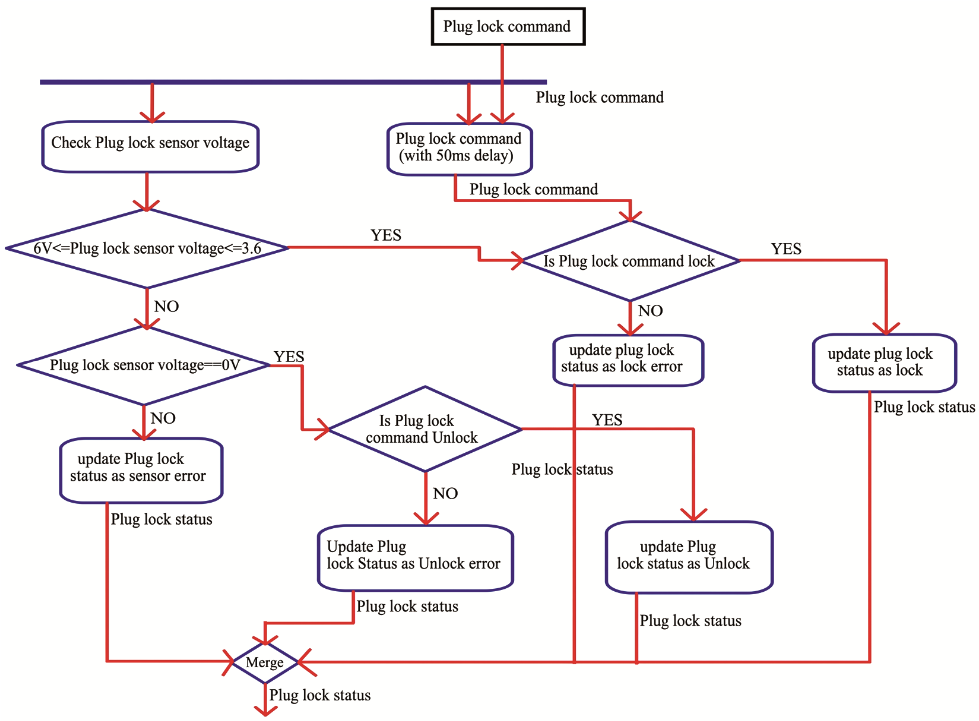

Fig. 16 — Plug lock status determination

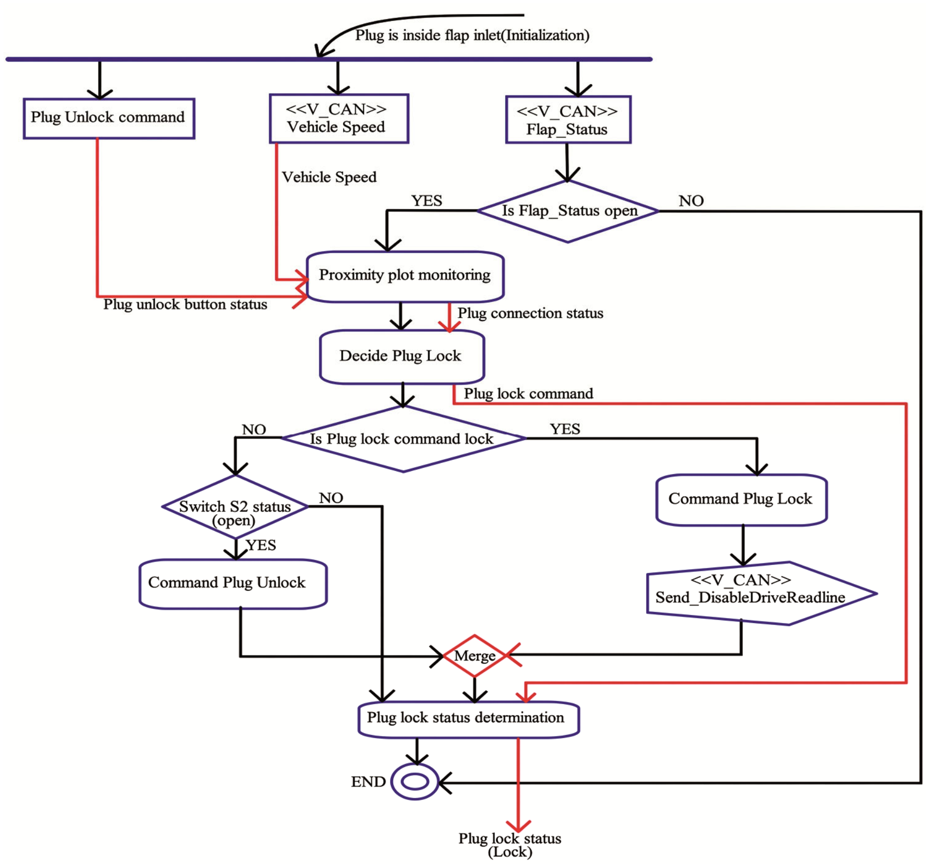

Fig. 17 — Charging Interface

Once charging begins, the OBC transitions to the ACTIVE state, performing its normal charging operations. If a fault occurs during this process and a derating_ongoing signal is received via the internal CAN (ICAN) network, the OBC shifts from ACTIVE to the DERATING state. In this mode also referred to as the DEGRADED state the OBC continues charging but at significantly reduced current and voltage levels to protect system components.

If CAN communication fails during charging, the OBC transitions to the CRASH state, indicating a critical fault that halts all charging operations. Figures 18 and 19 shows the ECU state behaviour of RH850 E2M MCB and the state behaviour of OBC that an OBC will undergo during charging.

5 System Modeling

A conventional Boost PFC is divided into two stages: the first one is a full-bridge rectifier that converts the AC supply voltage into DC. The second one is the Boost DC-DC converter that boosts up the DC-supply coming from the rectifier to the desired value.

5.1 Full Bridge Rectifier

One of the most used AC-DC converters for low-power applications is the full-wave rectifier. Figure 20 (a) illustrates a basic diode bridge rectifier without any filtering components. The operation is straightforward: during the positive half-cycle of the AC input, diodes D1 and D2 conduct, while during the negative half-cycle, diodes D3 and D4 conduct. This allows current to flow in the same direction through the load during both halves of the AC cycle.

Figure 20 (b) shows the output voltage waveform of the rectifier. In this configuration, the rectifier presents a resistive load to the AC source, resulting in

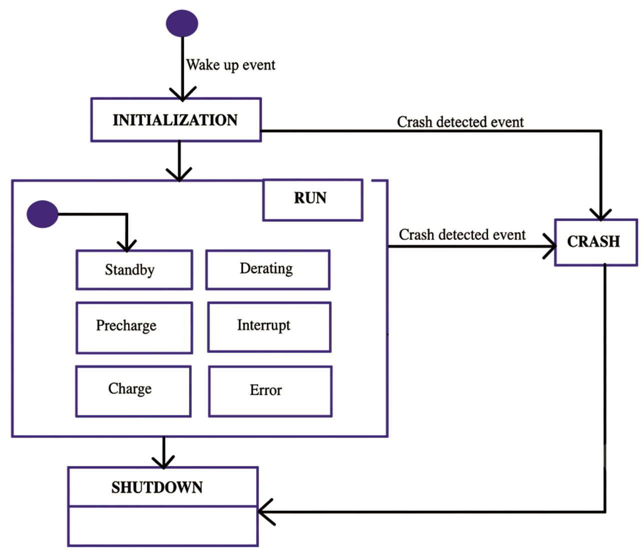

Fig. 18 — ECU state behavior of RH850 E2M MCB

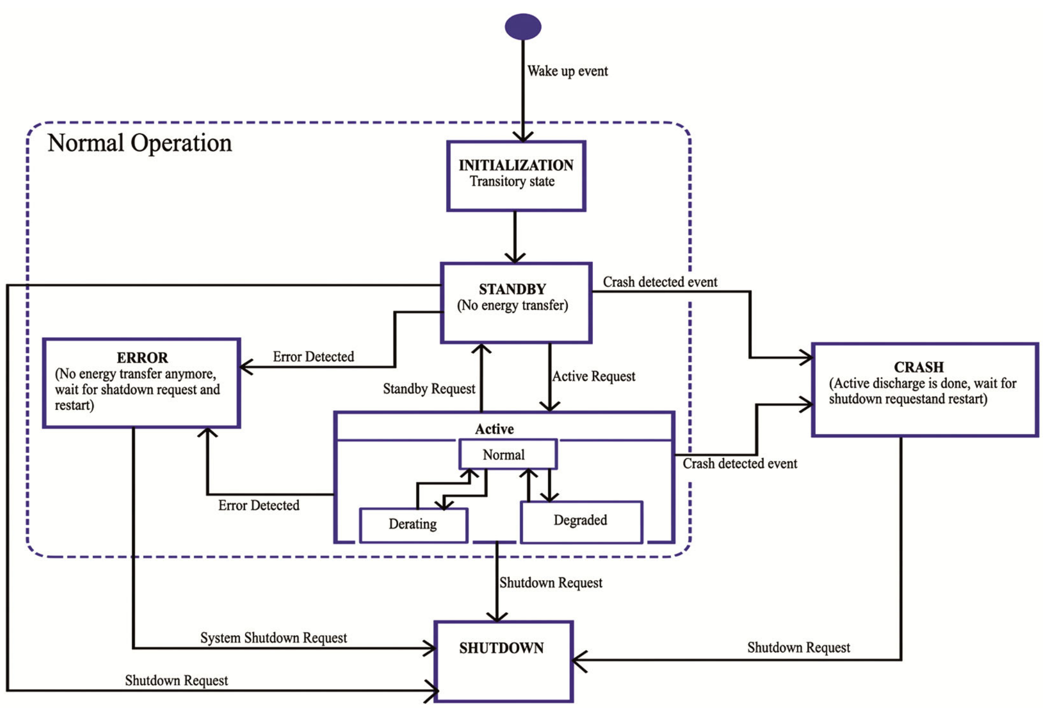

Fig. 19 — OBC state behavior

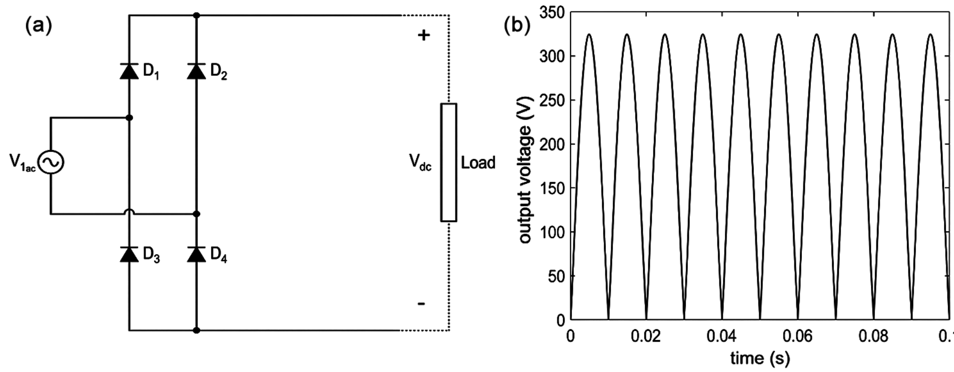

Fig. 20 — Diode bridge rectifier (a) power stage diagram; and (b) output voltage (*V*s=230 V RMS)

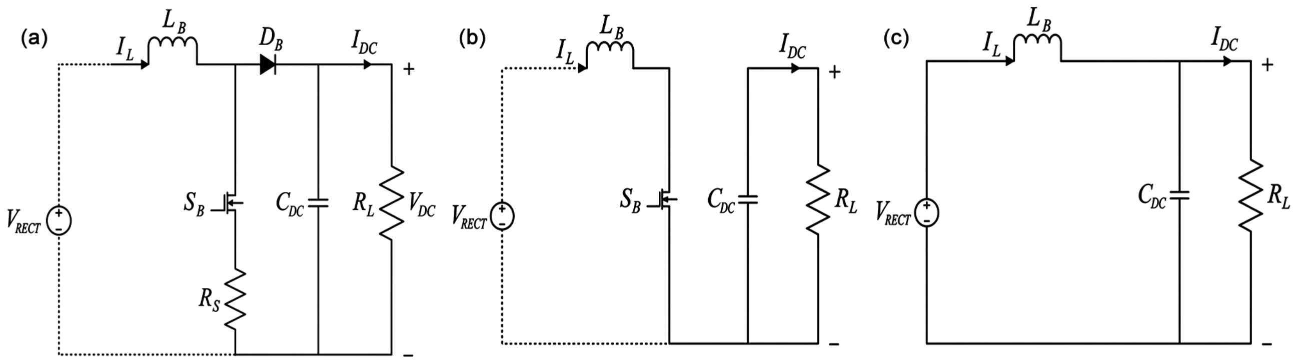

Fig. 21 — (a) Equivalent circuit of boost converter during (b) ON interval; and (c) OFF interval

the input current being in phase with the input voltage. This characteristic enables near-unity power factor operation, which is desirable for efficient energy conversion and minimal reactive power loss.

5.2 Boost DC-DC Converter

The input to Boost DC-DC converter is the rectified DC output of full bridge rectifier. This DC voltage is pulsating in nature varying from zero to peak value of the supply voltage. But for analysis and operation of boost converter, this pulsating DC voltage is assumed to be constant. The circuit configuration for both ON and OFF equivalent circuits is shown in Fig. 21.

During time interval 0 ≤ t ≤ TON, the boost switch SB is turned ON by gate pulse. At this interval, the boost inductor LB is short-circuited via switch SB and input voltage VRECT. The boost diode is reverse biased, and the load is supplied by the DC link capacitor. By applying Kirchhoff's voltage law and Kirchhoff's current law, the inductor voltage VL, capacitor current IC and capacitor voltage VC is given by Eqs. (4) – (6).

$$V_L = V_{RECT} \quad \dots (4)$$

$$I_C = -I_{DC} \quad \dots (5)$$

$$V_C = V_{DC} \quad \dots (6)$$

During time interval TON ≤ t ≤ TS, where TS is the total switching time of switch SB, boost switch SB is turned off with boost diode is in forward bias condition. By applying Kirchhoff's voltage law and Kirchhoff's current law, again the capacitor current IC and inductor voltage VL is given by Eqs. (7) and (8).

$$I_C = I_L - I_{DC} \quad \dots (7)$$

$$V_L = V_{RECT} - V_{DC} \quad \dots (8)$$

So, from the voltage-second balance in case of the inductor, from Eq. (9)

$$\int dI_L = \frac{1}{L}\int V_L dt = 0 \quad \dots (9)$$

or

$$V_{RECT} \times T_{ON} + (V_{RECT} - V_{DC})(T_S - T_{ON}) = 0$$

or

$$V_{DC} = \frac{V_{RECT}}{\frac{T_{OFF}}{T_S}} \quad \dots (10)$$

or

$$V_{DC} = \frac{V_{RECT}}{(1-D)} \quad \dots (11)$$

Equation (11) gives the final boosted DC output voltage from a conventional boost converter. In

Eq. (10), TOFF = TS-TON and in Eq. (11) D defines the duty cycle such that $0 \leq D \leq 1$.

5.3 Proportional-Integral Controller (PI control)

In a boost converter, the PI controller plays a crucial role in regulating the output voltage delivered to the load. By adjusting the integral gain (KI), the controller can reduce the system's time rise and eliminate steady-state error. However, increasing KI excessively may lead to system instability and a higher overshoot. Therefore, KI must be carefully tuned to balance fast response, minimal overshoot, and overall system stability.

In this design, the PI controller is used to generate PWM signals for controlling the switching of the MOSFET in the boost converter. The reference voltage (Vref) represents the desired DC output voltage, while the input voltage (Vg) is derived from the output of a full-wave rectifier. The controller continuously monitors the error signal (e), which is the difference between Vref and the actual output voltage. The control action persists until the error converges to zero, ensuring the system reaches its set point. This closed-loop control mechanism enables precise voltage regulation and enhances the performance of the DC-DC boost converter in the OBC system. For ON-state of the boost converter and by using Laplace transform.

$$V_g(s) = L \times S \times I_S(s) \quad \ldots (12)$$

where Is(s) is grid input current in the Laplace domain.

Also, again

$$V_o(s) = I_s(s) \times R \quad \ldots (13)$$

Therefore, the basic output transfer function of the converter.

$$\frac{V_g(s)}{V_o(s)} = \frac{L \times s}{R} \quad \ldots (14)$$

The output Vo(s) is sent to PWM, the output of which is compared with the PI controller. Vg is then added and given to the system.

$$V_o(s) = \frac{R}{L \times s}\left[V_g + \left(K_P + \frac{K_I}{s}\right) \times e\right] \quad \ldots (15)$$

Considering Vref = 0, the overall transfer function for PFC converter is given by (16).

$$\frac{V_o(s)}{V_{in}(s)} = \frac{\frac{R}{L \times s}}{\left[1 + \left(\frac{R}{L \times s}\right) \times \left(K_P + \frac{K_I}{s}\right) \times \left(\frac{1}{1-D}\right)\right]} \quad \ldots (16)$$

6 System Design

The designing must be done on MATLAB Simulink software using simscape tool. Table 2 shows the design specifications and parameters that are used for the design of the PFC converter.

It is essential to calculate the values of inductance and capacitance for determining the design parameters using the following Eqs. (17) and (18).

$$L = \frac{R \times D \times (1-D)^2}{2 \times f_{sw}} \quad \ldots (17)$$

where R is load resistance, D is the duty cycle and fsw is the switching frequency.

$$C = \frac{V_o \times D}{f_{sw} \times \Delta V \times R} \quad \ldots (18)$$

where, Vo is the output voltage, ΔV is output voltage ripples on the load side. The output voltage ripple is calculated before the design of the capacitive filter at the output side of PFC. As explained above PI control algorithm is used for PWM switching of MOSFET in PFC control design. The tuning parameters for the PI controller are selected by using the Ziegler-Nichols technique. Table 3 shows the method for using tuning parameters for controller design using the Ziegler-Nichols method.

The ultimate gain Ku is the proportional gain for a marginally stable system where the controller has a response with sustained oscillations. In the PFC circuit, the PI controller shows its response with sustained oscillations at Ku = 0.6 with a time period of oscillation Tu = 0.347 ms. Table 4 shows the value of tuning

Table 2 — Specifications for PFC converter

	Min	Nominal	Max
Input voltage[V]	-	120	-
Output voltage[V]	211	212	215
Inductor[mH]	-	2.5	-
Capacitor[µF]	-	1.689	-
Resistor[Ω]	-	200	-
Duty cycle [%]	-	50	-
Expected efficiency [%]	-	77.8	-
Switching frequency [KHz]	-	50	-
Input current[A]	-	2.61	-
Output current[A]	1.47	1.5	1.53
Output Power[watts]	-	243.6	-
Output voltage ripple[V]	-	6.067	-
Real power (P)[watts]	-	294.6	-
Apparent power(S)[watts]	-	313.1	-

Table 3 — Ziegler-Nichols (Z-N) Method

Controller Type	K_P	K_I	K_D
Proportional control (P)	$K_u/2$	-	-
Proportional integral (PI)	$K_u/2.2$	$1.2K_P/T_u$	-
Proportional integral Derivative (PID)	$0.6K_u$	$2K_P/T_u$	$K_PT_u/8$

Table 4 — Tuning parameters for PI control using Z-N method

Controller Type	K_P	K_I	K_D
Proportional Integral (PI)	0.27	9.337	-

parameters that have been obtained using the Z-N method.

7 Results

The MATLAB-based modeling and Simulink analysis of the OBC are categorized into two main stages. In the first stage, individual components of the OBC are modeled and simulated. This includes an AC-DC converter integrated with Active PFC, followed by a DC-DC converter equipped with voltage and current control mechanisms to support both Constant Voltage and Constant Current charging modes. In the second stage, the CC/CV charging profile of a lithium-ion battery used in electric vehicles is demonstrated using a half-bridge DC-DC converter. The simulation setup utilizes a 48V DC input supply, with a filter inductance of 5.7 μH serving as the primary energy storage element. This configuration ensures smooth current flow and stable voltage regulation during the charging process. Final fabricated prototype of the proposed antenna along with SMA cable and connector is shown in Fig. 22.

Figures 23 and 24 shows the MATLAB Simulink model for Active PFC and PI control algorithm that is used to generate PWM pulses. With this controller, a power factor, pf = 0.94 is achieved which is nearer to unity.

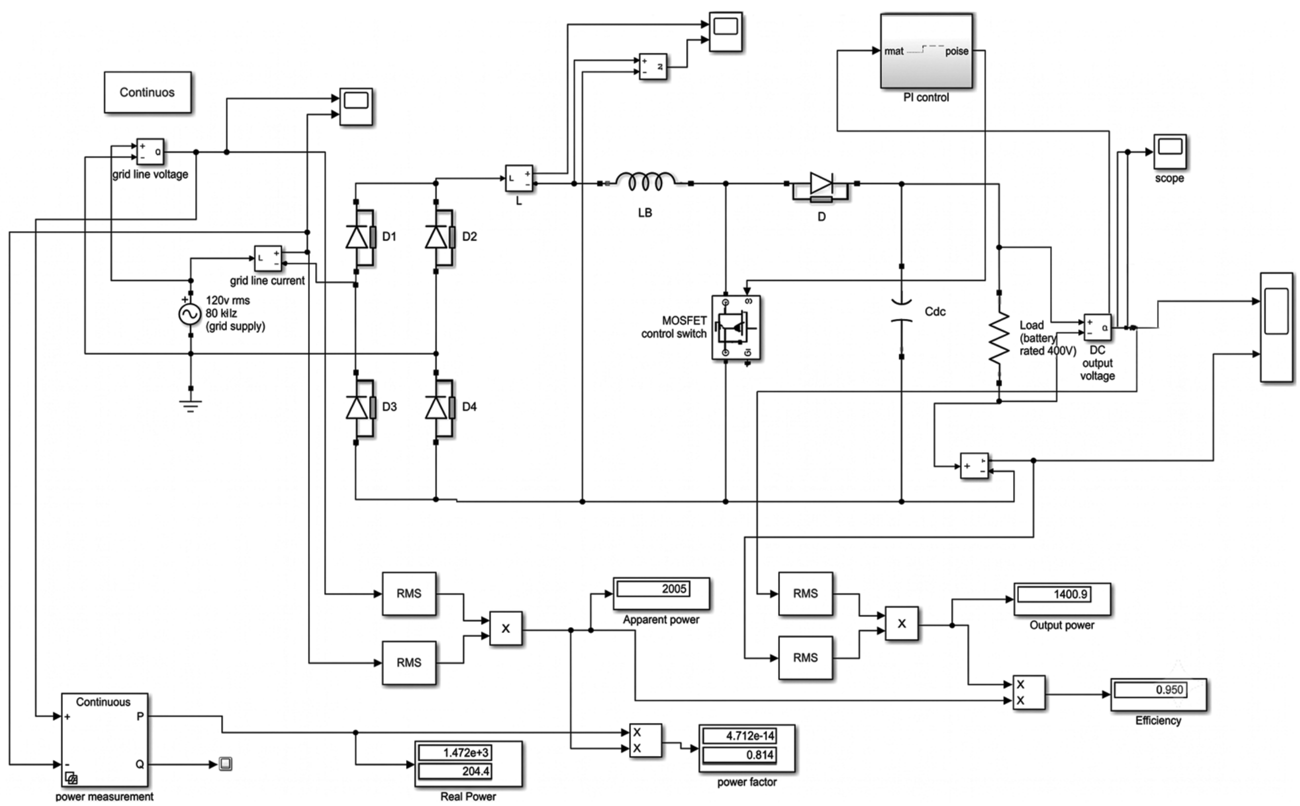

Fig. 22 — Final fabricated prototype of the proposed antenna along with SMA cable and connector

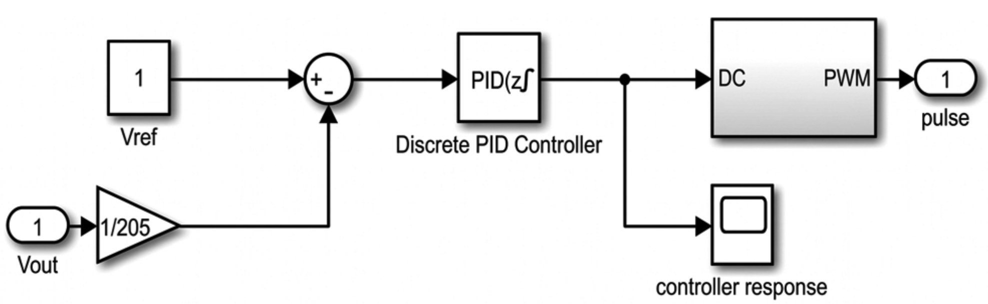

Fig. 23 — The PI control algorithm for Active PFC

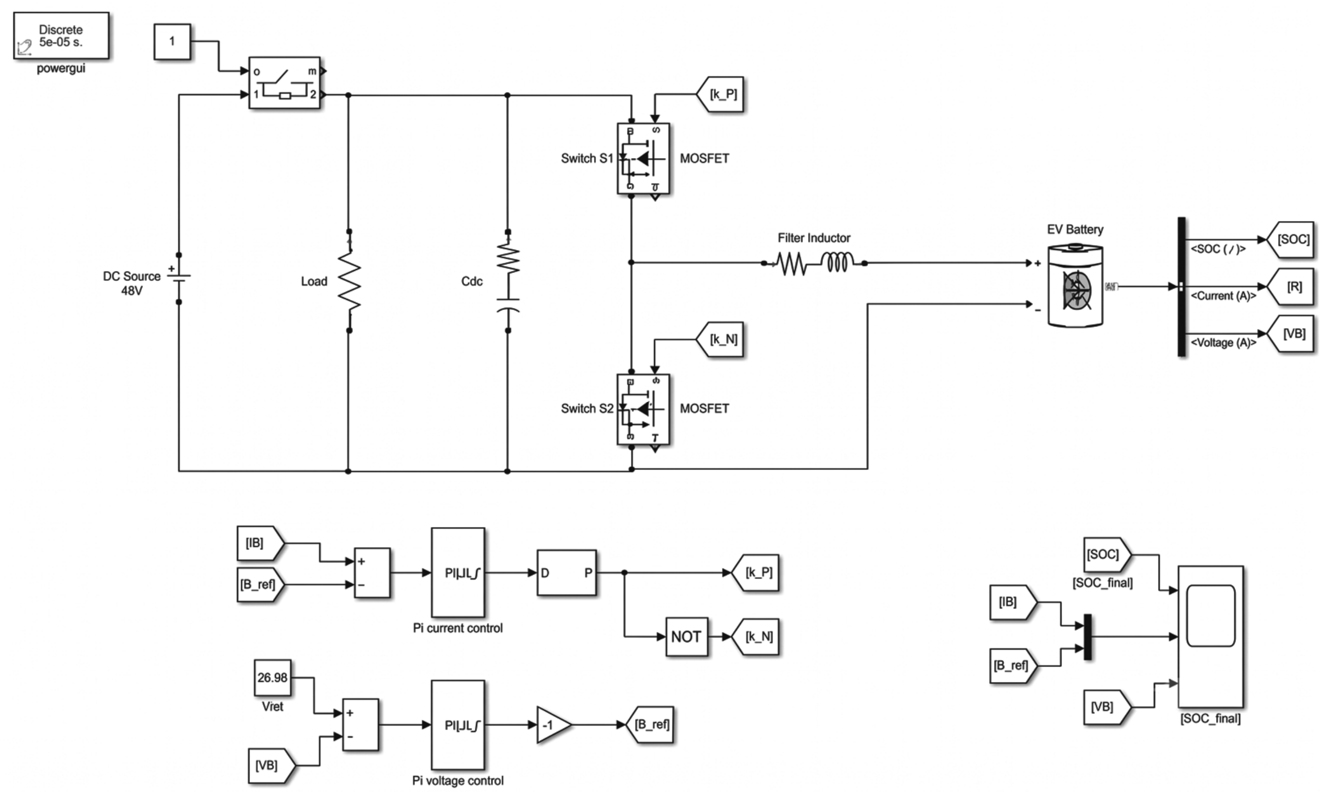

Fig. 24 — Comparison of simulated and measured S11 (dB) of proposed antenna

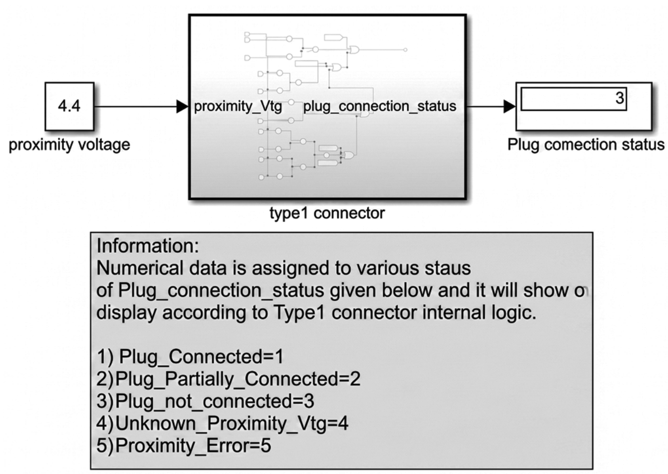

Fig. 25 — PPM subsystem for Type 1 connector

Figures 25 and 26 shows the MATLAB logical model for proximity pilot monitoring for Type 1 connector of standard SAEJ1772.

Proposed MATLAB logical model for switch S2 control is shown in Fig. 27. Proposed Plug lock status subsystem is given in Fig. 28 and Proposed logic for Plug lock status subsystem is shown in Fig. 29. Switch S2 is a key component within the Control Pilot ECU module, which plays a crucial role in managing the communication and charging phases between the EV and EVSE. As previously discussed, the control pilot circuit defines various charging states based on voltage levels, representing the EV and EVSE status. The charging process is initiated when Switch S2 is closed within the control pilot circuit. This occurs when the CP voltage falls within the range of 5V to 7V. Upon detecting this voltage range, the Microcontroller-Based Control Block issues a command

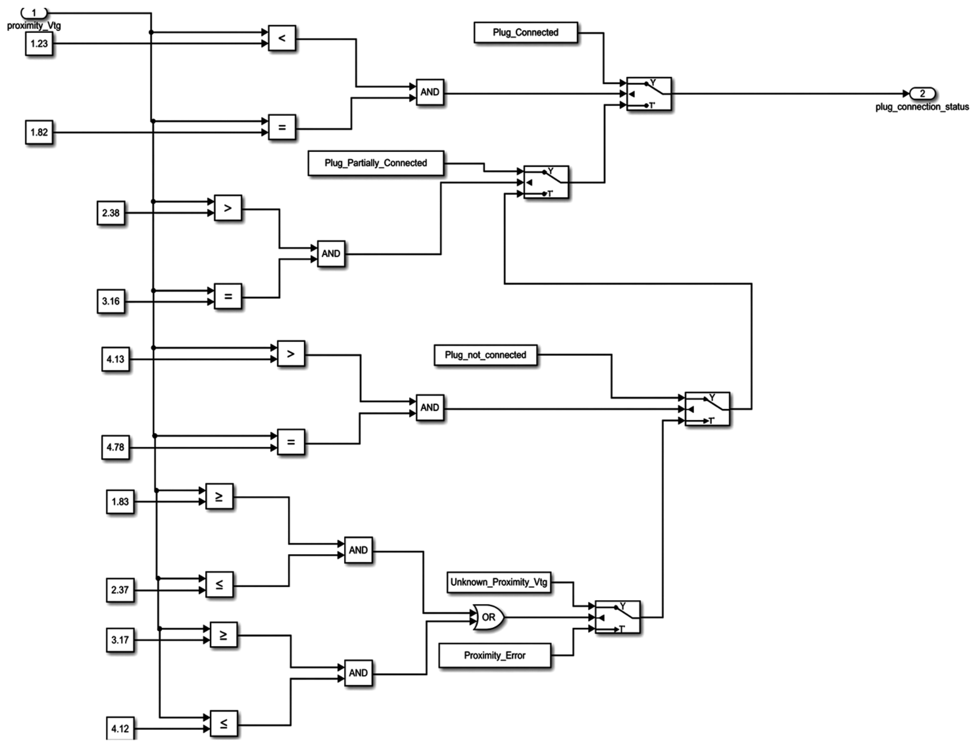

Fig. 26 — Internal logic for PPM subsystem

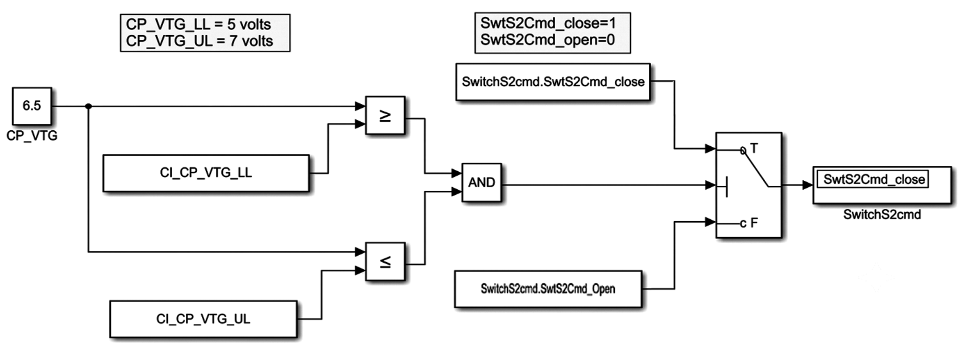

Fig. 27 — Proposed MATLAB logical model for Switch S2 control[16]

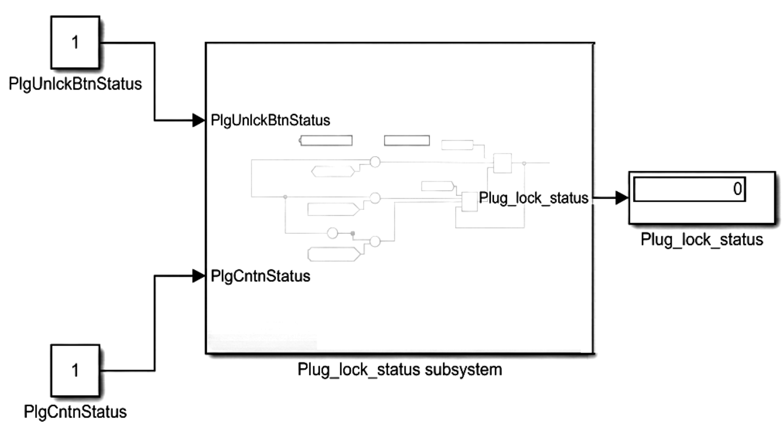

Fig. 28 — Proposed Plug lock status subsystem[16]

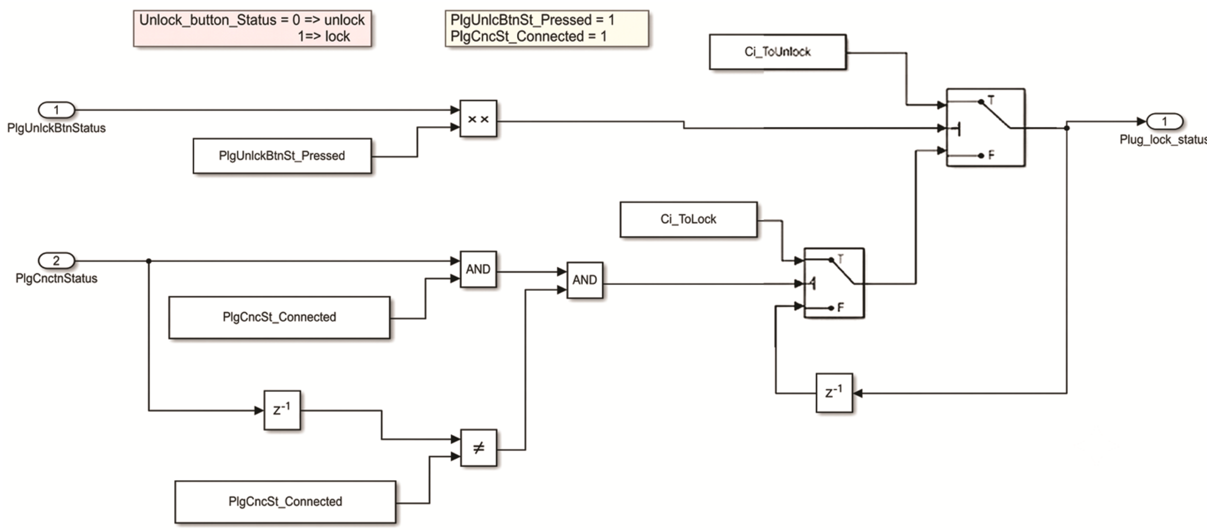

Fig. 29 — Proposed logic for Plug lock status subsystem[16]

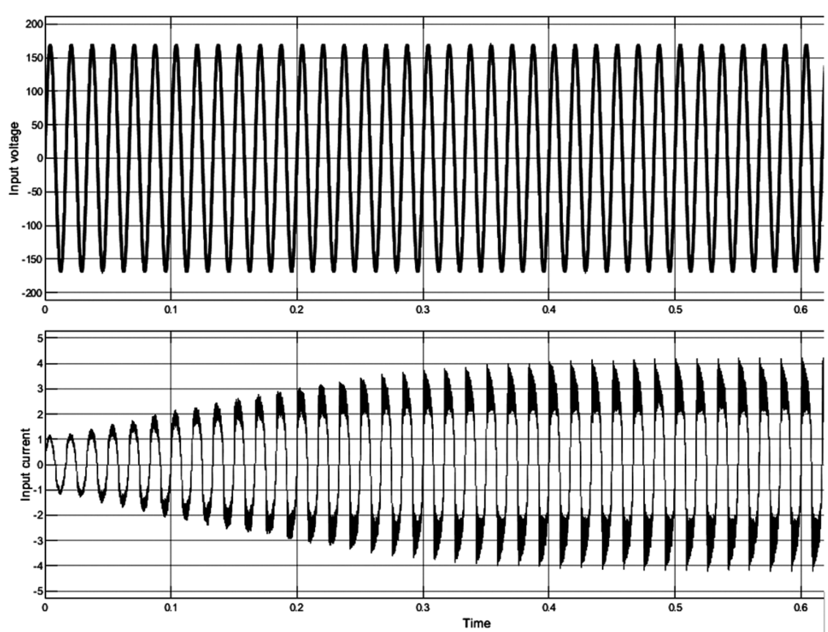

Fig. 30 — Internal logic for PPM subsystem[16]

to close Switch S2, thereby enabling the transition to the active charging state.

Internal Logic for PPM subsystem is shown in Fig. 30. Simulated line voltage and line current waveform operated at 120V RMS. The power factor is obtained as 0.94 with the circuit running at a duty cycle of 50 % and efficiency is found to be 77.8 %. The simulation of the model was done for t = 0.8 sec. The results are tabulated in Table 5.

The second phase of designing of OBC is to design DC-DC converter. For that the same conventional DC-DC boost converter which is simulated above followed by an inverter circuit with or without isolation. Since the output obtained from PFC is a dc voltage with ripples like full-wave rectifier output, this dc voltage can be boosted up by using a boost

Table 5 — Results obtained after simulation of PFC

Sr	Variables	Values
1	Output Power[watts]	243.6
2	Real Power[watts]	294.6
3	Apparent Power[watts]	313.1
4	Power factor(pf)	0.94
5	Efficiency (%)	77.8

converter to a voltage level as demanded by load battery present inside EV. The most preferred inverter that can be used in the middle phase is a Full bridge converter with IGBT switches and a transformer for providing isolation.

8 Conclusion

This paper proposes a systematic design approach for an OBC used in EVs. The initial phase involves analyzing the topologies of the two primary circuit stages the PFC stage and the DC-DC converter stage. Three topologies are evaluated for each stage based on their power efficiency, voltage regulation capabilities, and associated losses during operation.

For the PFC stage, Boost PFC, Interleaved Boost PFC, and Semi-bridgeless PFC are considered. Among these, the conventional Boost PFC is selected as the reference design due to its lower switching and conduction losses, involving only one switch and one diode. For the DC-DC converter stage, Full-Bridge, SRC, and Phase-Shift Full-Bridge topologies are discussed. To automate the switching operations, a PI controller is integrated into the circuit design. Further automation is introduced through the incorporation of the Renesas RH850 E2M microcontroller, which manages both hardware and software ECU modules and enables smart charging features.

Finally, a complete OBC model is developed using MATLAB Simulink, featuring a conventional Boost PFC and Boost DC-DC converter controlled via a PI algorithm. The model also includes logical representations of selected ECU software modules, making the OBC system compliant with the RH8. It can be used in defense applications also.

As the global EV market continues to expand rapidly driven by efficient energy usage and zero-emission benefits, countries involved in EV manufacturing and adoption are increasingly shifting their business strategies and policies toward EVs. This trend strongly indicates that the EV market is poised to reach its peak in the coming years.

From a technical standpoint, the EV charging process involves complex switching operations across both stages of the OBC. These operations are inherently non-linear, making them suitable for advanced control strategies such as Sliding Mode Control or Linear Quadratic Regulator (LQR) control. Implementing these techniques can help generate precise PWM signals, enhancing overall system performance and efficiency.

Additionally, the Renesas RH850 E2M microcontroller offers robust support for smart charging. It can manage up to four OBC and DC-DC converter units simultaneously and is compatible with various ECU software modules, including error handling, control pilot monitoring, maximum line current regulation, and mode management. These features contribute to a more intelligent and reliable charging process. With such advancements in automotive electronics and control systems, EVs are not only becoming essential to the future of the automotive industry but are also contributing to improved quality of life and environmental sustainability.

References

1 Kumar N & Prasad M P R, A comparative analysis of different topologies of on-board charger (OBC) with an approach of interfacing it with MCB, *Proc 6th Int Conf Convergence Technol* (I2CT) (2021).

2 Koo K W, Kim D H & Woo D G, Topology comparison for 6.6 kW on-board charger: Performance, efficiency, and selection guideline, *Proc IEEE Vehicle Power Propulsion Conf (VPPC),* Seoul, Korea (2012).

3 Kumar N, Design and analysis of MCB compliant on-board charger on the basis of topologies, efficiency, losses and automation, (2020) 45.

4 Sung W Y, Oh C Y, Kim Y S & Lee B K, Design of system efficiency analysis platform using PSIM MATLAB simulation, *Proc KIEE* (2011).

5 Asim M, Parveen H, Mallick M A & Siddiqui A, *Int J Innov Res Electr Electron Instrum Control Eng*, 3 (2015) (11) 107.

6 Kazmierkowski M P*,* Direct power control of three-phase PWM rectifier using space vector modulation-simulation study, *Proceedings of the 2002 IEEE International Symposium*, 4 (2002) 1114.

7 Bildirici M & Karaarslan A, Analysis of Cuk converter using PI and OCC control method, *Proc ICTPE Conf* (2017).

8 Mohanty P, Power factor correction of AC–DC system using boost converter, 1 (2014) 23.

9 Mohanty N R, Design and analysis of an on-board electric vehicle charger for wide battery voltage range, 2 (2016) 19.

10 Electric Vehicle Conductive DC Charging System, *Automotive Research Association of India*, *AIS (*138) Part 2, (2018) 64.

11 Hanchour K M & Benahmed B, *Int J Math Model Numer Optim*, 13 (2023) 123.

12 Grenier, Aghdam M, Hosseini M G & Thiringer, Design of on-board charger for plug-in hybrid electric vehicle, *IEEE Trans Power Electron*, 28 (5) (2013) 231.

13 Kushwahi M & Patra A, *Int J Sci Eng Technol Res*, 3 (13) (2018) 8.

14 Gowrishankar J, Balasundaram G, Manikandan J, Chandrakala D & Munisekhar P, *Int J Math Model Numer Optim*, 13 (2023) 350.

15 Boindala S P, Arunachalam V & Christopher J J, *Int J Math Model Numer Optim*, 14 (2024) 1.

16 Rajeshkumar Patel N, Analysis and Design of Soft-Switching Current-fed Bi-directional Power Conversion for Multifunctional Plug-in EV Charging, (2024).